

Electric dipole radiation near a mirror

Xin Li* and Henk F. Arnoldus†

Department of Physics and Astronomy, Mississippi State University, P. O. Drawer 5167, Mississippi State, Mississippi 39762–5167, USA

(Received 5 February 2010; published 24 May 2010)

The emission of radiation by a linearly oscillating electric dipole is drastically altered when the dipole is close to the surface of a mirror. The energy is not emitted along optical rays, as for a free dipole, but as a set of four optical vortices. The field lines of energy flow spiral around a set of two lines through the dipole. At a larger distance from the dipole, singularities and isolated vortices appear. It is shown that these interference vortices are due to the vanishing of the magnetic field at their centers. In the plane of the mirror there is a singular circle with a diameter which is proportional to the distance between the dipole and the mirror. Inside this circle, all energy flows to a singularity on the mirror surface.

DOI: [10.1103/PhysRevA.81.053844](https://doi.org/10.1103/PhysRevA.81.053844)

PACS number(s): 42.25.Gy, 42.25.Hz

I. INTRODUCTION

When a small source of radiation is located near an interface, the emitted light that propagates toward the surface partially reflects and partially refracts at the boundary. We consider the case where the medium is a perfect mirror, so that all light reflects. The angle of reflection of an optical ray is equal to the angle of incidence, and by considering the path of two rays, as in Fig. 1(a), it appears that a virtual image is formed below the mirror such that the distance between the object and the mirror is equal to the distance between the image and the mirror. Part of the emitted light travels directly from the source to an observer, and the result is that both the source and the image can be seen. Ray diagrams as in Fig. 1(a) are justified in the geometrical optics limit of light propagation [1] in which variations in the optical field on the scale of a wavelength are neglected. It is furthermore assumed that the source is incoherent, so that any interference between optical rays washes out. In the geometrical optics limit, the rays are the orthogonal trajectories of the wave fronts, and for propagation in vacuum it can then be shown that the rays are straight lines. The direction of energy flow in any radiation field is determined by the direction of the electromagnetic Poynting vector, and in the geometrical optics limit the field lines of the Poynting vector coincide with the optical rays. Therefore, in the geometrical optics limit, electromagnetic energy flows along straight lines, which are the optical rays.

When the source of radiation is an atom, a molecule, or a nanoparticle, for instance driven by a laser beam, the radiation can no longer be considered incoherent and there will be interference between the different paths of energy propagation. When the source near a mirror is viewed from the far field (many wavelengths away), an interference pattern will be observed, and the source and its image can no longer be distinguished. The ray diagram of Fig. 1(a) is still valid, although its interpretation is then derived from an angular spectrum representation of the source field and the reflected field. In this approach, the radiated electric and magnetic fields are represented by superpositions of traveling and evanescent plane waves [2–5]. In the far field, only the plane waves

survive, and it can be shown by asymptotic expansion of the angular spectrum with the method of stationary phase (Appendix III of Ref. [1]) that the interference pattern in the far field is consistent with the ray diagram of Fig. 1(a). For a coherent source, however, the rays in Fig. 1(a) are not the paths of energy propagation but rather visualizations of the wave vectors of the traveling waves in an angular spectrum representation.

In near-field optics and nanophotonics, variations in the optical field on the scale of a wavelength are of interest and objects may be located at a subwavelength distance from an interface. Then the geometrical optics limit breaks down, whether the source is coherent or not. When measurements are performed in the near field, an interpretation of the ray diagram of Fig. 1(a) also loses its significance in terms of the angular spectrum, since the near field is dominated by the evanescent waves. In any case, when subwavelength phenomena are of interest, the exact solution of Maxwell's equations has to be adopted. The paths of energy flow are the field lines of the Poynting vector, and usually these field lines are curves rather than straight lines. Field lines of any vector field cannot cross, whereas the optical rays in Fig. 1(a) do cross. So when considering the flow of energy out of a source near a mirror, we expect a smooth flow pattern as in the sketch in Fig. 1(b). Near the interface, the Poynting vector is tangential to the boundary, as follows from the boundary conditions of Maxwell's equations, and therefore the field lines reflect smoothly at the mirror. This is in contrast to the reflection in the ray diagram in Fig. 1(a), where the rays make a sharp turn at the interface.

For the construction of the image with a ray diagram, as in Fig. 1(a), the details of the source are irrelevant, whereas for the flow line diagram in Fig. 1(b), the details of the flow pattern depend on the precise structure of the source. We consider the emission of radiation by a harmonically oscillating linear dipole near a mirror. It turns out that the flow line picture is generally far more complicated than that suggested in Fig. 1(b), and we also show that the process of emission of radiation is drastically altered due to the presence of the mirror.

II. ELECTRIC DIPOLE RADIATION

The radiation emitted in electronic transitions in atoms or molecules is usually electric dipole radiation, and the scattered

*x1121@msstate.edu

†hfa1@msstate.edu

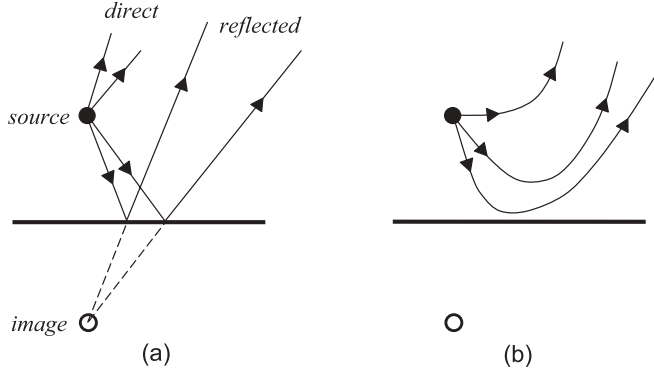


FIG. 1. (a) In the geometrical optics limit of light propagation, the mirror image of an incoherent point source can be constructed by considering the reflection of the optical rays. (b) For the exact solution of Maxwell's equations, the flow of energy is determined by the field lines of the Poynting vector. In contrast to the optical rays, these field lines are smooth curves.

light by a nanoparticle in a laser beam is in first approximation electric dipole radiation. When light with angular frequency ω is emitted, the electric field can be written as

$$\mathbf{E}(\mathbf{r}, t) = \text{Re}[\mathbf{E}(\mathbf{r})e^{-i\omega t}], \quad (1)$$

where $\mathbf{E}(\mathbf{r})$ is the complex amplitude, and the emitted magnetic field $\mathbf{B}(\mathbf{r}, t)$ can be represented similarly. A linear electric dipole has a dipole moment of the form

$$\mathbf{d}(t) = d_0 \boldsymbol{\varepsilon} \cos(\omega t), \quad (2)$$

where $\boldsymbol{\varepsilon}$ is a unit vector. This dipole moment oscillates with amplitude d_0 along an axis represented by vector $\boldsymbol{\varepsilon}$. For a dipole located at the origin of coordinates, the complex amplitudes of the electric and magnetic fields are given by [6]

$$\mathbf{E}(\mathbf{r}) = \frac{k_0^3 d_0}{4\pi \varepsilon_0 q} \left\{ \boldsymbol{\varepsilon} - (\boldsymbol{\varepsilon} \cdot \hat{\mathbf{r}}) \hat{\mathbf{r}} + [\boldsymbol{\varepsilon} - 3(\boldsymbol{\varepsilon} \cdot \hat{\mathbf{r}}) \hat{\mathbf{r}}] \frac{i}{q} \left(1 + \frac{i}{q} \right) \right\} e^{iq}, \quad (3)$$

$$\mathbf{B}(\mathbf{r}) = -\frac{k_0^3 d_0}{4\pi \varepsilon_0 c q} \boldsymbol{\varepsilon} \times \hat{\mathbf{r}} \left(1 + \frac{i}{q} \right) e^{iq}. \quad (4)$$

Here, $\hat{\mathbf{r}}$ is the unit vector into the direction of observation, $k_0 = \omega/c$ is the wave number in free space, and we have set $q = k_0 r$ for the dimensionless distance between the dipole and the field point. On this scale, a dimensionless distance of 2π corresponds to one optical wavelength.

The energy flow in an electromagnetic field is determined by the Poynting vector $\mathbf{S}(\mathbf{r}, t)$. The direction of \mathbf{S} is the direction of energy flow, and the magnitude of \mathbf{S} equals the power through a unit area, perpendicular to \mathbf{S} . For a time-harmonic field, $\mathbf{S}(\mathbf{r}, t)$ is independent of time and given by

$$\mathbf{S}(\mathbf{r}) = \frac{1}{2\mu_0} \text{Re}[\mathbf{E}(\mathbf{r}) \times \mathbf{B}(\mathbf{r})^*]. \quad (5)$$

This is the time-averaged Poynting vector, in which terms that oscillate at twice the optical frequency have been dropped, since these average to zero on the time scale of an optical cycle. With expressions (3) and (4) we then obtain

$$\mathbf{S}(\mathbf{r}) = \frac{3P_0}{8\pi r^2} \hat{\mathbf{r}} \sin^2 \alpha, \quad (6)$$

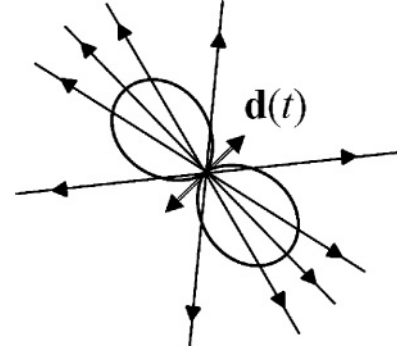


FIG. 2. Field lines of the Poynting vector for a linear dipole with dipole moment $\mathbf{d}(t)$, and a polar plot of the power per unit solid angle.

where

$$P_0 = \frac{ck_0^4}{12\pi \varepsilon_0} d_0^2 \quad (7)$$

equals the total radiated power by the dipole. Angle α in Eq. (6) is the angle between vector $\boldsymbol{\varepsilon}$ and the observation direction $\hat{\mathbf{r}}$. The Poynting vector is proportional to $\hat{\mathbf{r}}$ for all field points \mathbf{r} , and therefore the field lines of $\mathbf{S}(\mathbf{r})$ are straight lines which run radially outward from the location of the dipole. The emitted power per unit solid angle, $dP/d\Omega$, is equal to $r^2 \mathbf{S}(\mathbf{r}) \cdot \hat{\mathbf{r}}$, so that

$$\frac{dP}{d\Omega} = \frac{3P_0}{8\pi} \sin^2 \alpha. \quad (8)$$

Figure 2 shows the field lines of the Poynting vector for a free linear dipole, and a polar diagram of the power per unit solid angle. No radiation is emitted along the dipole axis ($\alpha = 0$), and the field lines are drawn more densely in the directions of the extrema of the lobes ($\alpha = \pi/2$). In a three-dimensional (3D) view, the diagram is rotationally symmetric around the dipole axis.

III. DIPOLE RADIATION NEAR A MIRROR

We now consider the dipole located on the z axis, a distance H above a mirror, and the surface of the mirror is taken as the xy plane. The position vector of the dipole is given by $H\mathbf{e}_z$, and when we let \mathbf{r}_1 be the location of a field point with respect to the position of the dipole, then the position vector of that field point with respect to the origin is given by $\mathbf{r} = H\mathbf{e}_z + \mathbf{r}_1$. The setup is illustrated in Fig. 3. The complex amplitudes $\mathbf{E}(\mathbf{r})_s$ and $\mathbf{B}(\mathbf{r})_s$ of this source are given by Eqs. (3) and (4) with the replacements $\hat{\mathbf{r}} \rightarrow \hat{\mathbf{r}}_1$, the unit vector in the \mathbf{r}_1 direction, and $q \rightarrow q_1 = k_0 r_1$, the dimensionless distance between the dipole and the field point. The y axis is taken such that the dipole vector $\boldsymbol{\varepsilon}$ is in the yz plane. The dipole axis makes an angle γ with the z axis and, therefore, vector $\boldsymbol{\varepsilon}$ is

$$\boldsymbol{\varepsilon} = \mathbf{e}_y \sin \gamma + \mathbf{e}_z \cos \gamma. \quad (9)$$

The field reflected by the mirror is identical to the field of an image dipole [7] located at $-H\mathbf{e}_z$ and with dipole moment $d_0 \boldsymbol{\varepsilon}^{\text{im}} \cos(\omega t)$, where

$$\boldsymbol{\varepsilon}^{\text{im}} = -\mathbf{e}_y \sin \gamma + \mathbf{e}_z \cos \gamma. \quad (10)$$

The complex amplitudes $\mathbf{E}(\mathbf{r})_r$ and $\mathbf{B}(\mathbf{r})_r$ of the reflected field are as in Eqs. (3) and (4) with $\boldsymbol{\varepsilon} \rightarrow \boldsymbol{\varepsilon}^{\text{im}}$, $\hat{\mathbf{r}} \rightarrow \hat{\mathbf{r}}_2$, and

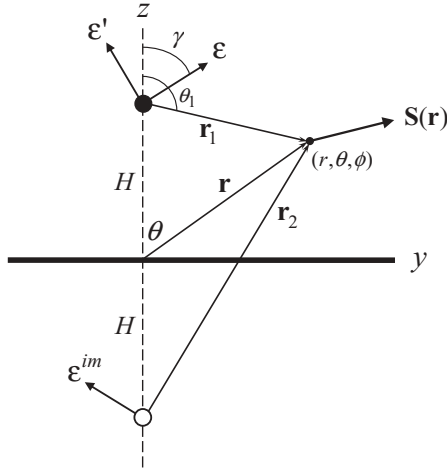


FIG. 3. A dipole is located on the z axis, a distance H above a mirror. The dipole oscillates along the direction indicated by vector $\boldsymbol{\epsilon}$, which makes an angle γ with the z axis. The reflected field is identical to the field of an image dipole, located at a distance H below the mirror, and on the z axis. The image dipole oscillates along the direction $\boldsymbol{\epsilon}^{im}$, which is also under angle γ with the z axis, but it has its horizontal component reversed as compared to $\boldsymbol{\epsilon}$. Vector $\boldsymbol{\epsilon}'$ is perpendicular to $\boldsymbol{\epsilon}$. A field point can be represented by vector \mathbf{r} with respect to the origin, or by vector \mathbf{r}_1 or \mathbf{r}_2 with respect to the dipole or the image dipole, respectively. A field point can also be represented by the spherical coordinates (r, θ, ϕ) with respect to the origin or the spherical coordinates (r_1, θ_1, ϕ) with respect to the position of the dipole.

$q \rightarrow q_2 = k_0 r_2$, and vector \mathbf{r}_2 is the position vector of the field point with respect to the location of the image dipole, as shown in Fig. 3. The total field in the region $z > 0$ is then the sum $\mathbf{E}(\mathbf{r}) = \mathbf{E}(\mathbf{r})_s + \mathbf{E}(\mathbf{r})_r$, $\mathbf{B}(\mathbf{r}) = \mathbf{B}(\mathbf{r})_s + \mathbf{B}(\mathbf{r})_r$. It can be verified explicitly that this field satisfies the boundary conditions for a perfect conductor at $z = 0$; e.g., the parallel part of $\mathbf{E}(\mathbf{r})$ and the perpendicular part of $\mathbf{B}(\mathbf{r})$ vanish.

With $\mathbf{E}(\mathbf{r})$ and $\mathbf{B}(\mathbf{r})$ constructed, the Poynting vector $\mathbf{S}(\mathbf{r})$ from Eq. (5) can be computed. The expression is rather lengthy and is given in Appendix A. The result for $\mathbf{S}(\mathbf{r})$ defines a vector field in space, and a field line of $\mathbf{S}(\mathbf{r})$ is a curve for which, at any point along the curve, the vector $\mathbf{S}(\mathbf{r})$ is on its tangent line. First, we set

$$\mathbf{S}(\mathbf{r}) = \frac{3P_0}{8\pi r_1^2} \boldsymbol{\sigma}(\mathbf{r}) \quad (11)$$

so that $\boldsymbol{\sigma}(\mathbf{r})$ is dimensionless. Since a field line is only determined by the direction of $\mathbf{S}(\mathbf{r})$ and not its magnitude, the field lines of $\boldsymbol{\sigma}(\mathbf{r})$ are the same as the field lines of $\mathbf{S}(\mathbf{r})$. For a field point \mathbf{r} we set $\mathbf{q} = k_0 \mathbf{r}$ for its dimensionless representation. Let $\mathbf{q}(u)$ be a parametrization of a field line, with u a dummy variable. The field lines $\mathbf{q}(u)$ are solutions of the autonomous differential equation

$$\frac{d\mathbf{q}}{du} = \boldsymbol{\sigma}(\mathbf{q}). \quad (12)$$

The field lines in the figures that follow are made by numerical integration of Eq. (12).

At the surface of the mirror, $\mathbf{E}(\mathbf{r})$ is perpendicular to the surface and $\mathbf{B}(\mathbf{r})$ is in the xy plane. It then follows from Eq. (5)

that $\mathbf{S}(\mathbf{r})$ is in the xy plane, and therefore any field line that approaches the mirror is expected to bend smoothly away from it, as suggested in Fig. 1(b).

IV. EMISSION OF RADIATION

For a free dipole the radiation is emitted in all directions, as shown in Fig. 2, and the Poynting vector is radially outward at any field point. We now consider the radiation field in close vicinity of the dipole for a dipole located near a mirror. We use spherical coordinates (r_1, θ_1, ϕ) with respect to the location of the dipole, and we set $q_1 = k_0 r_1$ for the dimensionless distance between the dipole and the field point. Both the electric and the magnetic fields of the source diverge when approaching the dipole. The electric field diverges as $O(1/q_1^3)$ and the magnetic field goes as $O(1/q_1^2)$, as follows from Eqs. (3) and (4), respectively. The reflected field appears to come from the image dipole, and close to the dipole both the electric and the magnetic fields (amplitudes) of the image dipole are finite at the location of the dipole. Therefore, the electric and magnetic fields close to the dipole are dominated by the field emitted by the source. One may therefore expect that close to the dipole the field lines of the Poynting vector come out of the dipole, as in Fig. 2, and at some distance from the dipole the reflected field becomes comparable to the source field, and interference sets in. This would then lead to a flow line pattern as sketched in Fig. 1(b). We now show that this is not the case.

The Poynting vector $\boldsymbol{\sigma}(\mathbf{q})$ [with a factor split off as in Eq. (11)] is given by Eq. (A11), and it has only γ and h , with $h = k_0 H$, as free parameters. The vector fields $\mathbf{S}(\mathbf{r})$ and $\boldsymbol{\sigma}(\mathbf{q})$ have the same field lines, so we only need to consider the vector fields $\boldsymbol{\sigma}(\mathbf{q})$. We consider the region close to the dipole, such that $q_1 \ll 1$ and $q_1 \ll h$. In physical terms, this means that we consider field points that are close to the dipole as compared to a wavelength, and we assume that the distance between the mirror and the dipole is much larger than the distance between the dipole and the field point. The Poynting vector $\boldsymbol{\sigma}(\mathbf{q})$ can be expanded in a series in q_1 , and it is shown in Appendix B that the result is

$$\boldsymbol{\sigma}(\mathbf{q}) = \frac{\sin \gamma}{q_1} v(h) [(3 \cos^2 \alpha - 1) \boldsymbol{\epsilon}' - 3 \cos \alpha (\hat{\mathbf{q}}_1 \cdot \boldsymbol{\epsilon}') \boldsymbol{\epsilon}] + \hat{\mathbf{q}}_1 \sin^2 \alpha + O(1). \quad (13)$$

Here we have introduced the function

$$v(h) = \frac{1}{2h} \left[\frac{\sin(2h)}{2h} - \cos(2h) \right], \quad (14)$$

and α is the angle between $\boldsymbol{\epsilon}$ and the observation direction $\hat{\mathbf{q}}_1$ (e.g., $\cos \alpha = \boldsymbol{\epsilon} \cdot \hat{\mathbf{q}}_1$), as in Eq. (6). Vector $\boldsymbol{\epsilon}'$ is defined as

$$\boldsymbol{\epsilon}' = -\mathbf{e}_y \cos \gamma + \mathbf{e}_z \sin \gamma. \quad (15)$$

This vector is perpendicular to $\boldsymbol{\epsilon}$ and is directed as shown in Fig. 3.

Without the mirror, the Poynting vector would be $\boldsymbol{\sigma}(\mathbf{q}) = \hat{\mathbf{q}}_1 \sin^2 \alpha$, as in Eq. (6), and in Eq. (13) this is the second term on the right-hand side. The corresponding field lines would run straight out from the dipole if this were the leading term at a close distance. In Eq. (13), however, the first term is $O(1/q_1)$, and for small enough q_1 this term dominates over the free-dipole term $\hat{\mathbf{q}}_1 \sin^2 \alpha$. Since this term is due to interference

between the source and the image field, we conclude that very close to the dipole the power flow is determined by interference rather than free emission. The term $\hat{\mathbf{q}}_1 \sin^2 \alpha$ is $O(1)$, as are the remaining terms of the expansion, but it is split off explicitly in Eq. (13) for the reasons below.

In the neighborhood of the dipole, the electric field is $O(1/q_1^3)$ and the magnetic field is $O(1/q_1^2)$. When computing the Poynting vector, this may seem to lead to $\mathbf{S}(\mathbf{r}) = O(1/q_1^5)$, with Eq. (5), and for $\sigma(\mathbf{q})$ this would be $O(1/q_1^3)$. However, the high-order terms cancel exactly and we get $\sigma(\mathbf{q}) = O(1)$ for a free dipole, which is the second term on the right-hand side of Eq. (13). The cross term between the electric field of the source, which is $O(1/q_1^3)$, and the magnetic field of the image, which is $O(1)$ at the location of the dipole, gives a contribution of $O(1/q_1)$ to $\sigma(\mathbf{q})$, and this is the first term on the right-hand side of Eq. (13). Consequently, sufficiently close to the dipole this interference term is larger than the source term $\hat{\mathbf{q}}_1 \sin^2 \alpha$.

The emission pattern of the radiation is determined by the energy flow lines in the immediate neighborhood of the source. In order to determine the structure of this pattern, we first consider a field point \mathbf{q}_1 in a plane through the dipole, which is perpendicular to vector \mathbf{e}' . For such a field point we have $\hat{\mathbf{q}}_1 \cdot \mathbf{e}' = 0$, and therefore the $O(1/q_1)$ term in Eq. (13) is proportional to \mathbf{e}' . Consequently, in this plane the Poynting vector $\sigma(\mathbf{q})$ is perpendicular to the plane, and the corresponding field lines cross the plane under a 90° angle. The factor of $3 \cos^2 \alpha - 1$, multiplying \mathbf{e}' , becomes zero when $\cos \alpha = \pm 1/\sqrt{3}$. Since α is the angle between \mathbf{e} and $\hat{\mathbf{q}}_1$, the condition $\cos \alpha = \pm 1/\sqrt{3}$ defines two lines in the plane on which the $O(1/q_1)$ contribution to the Poynting vector vanishes. These lines are under 54.7° with the \mathbf{e} axis and are indicated by ℓ_+ and ℓ_- in Fig. 4. Across these semisingular lines, the Poynting vector changes direction, leading to a rotation of the field lines around these lines in the plane. The orientation of the Poynting vector in this plane is shown in Figs. 4 and 5 shows several field lines resulting from this rotation. Apparently, when an oscillating electric dipole is located near a mirror, the radiation is emitted in a pattern of four vortices. Each field line swirls around one of the lines ℓ_+ and ℓ_- in the plane. Two vortices are in front of the yz plane, as shown in Fig. 5, and two are in the back. The Poynting vector is proportional to $v(h)$, which depends on the distance between the dipole and the surface of the mirror. When h changes, this function may change sign, and in that case the orientation of the rotation of the field lines around the semisingular lines reverses.

In Eq. (B4) of Appendix B, the $O(1)$ term of Eq. (13) is given explicitly, and we see that this term vanishes as $\sim 1/h$ for h large, except for the free-dipole part $\hat{\mathbf{q}}_1 \sin^2 \alpha$, which is independent of h . Therefore, for a field point on a semisingular line the Poynting vector is approximately equal to $(2/3)\hat{\mathbf{q}}_1$, for h not too small. On these lines the $O(1/q_1)$ term vanishes, but the Poynting vector is finite, and radially outward. From the diagram in Fig. 4 we can easily derive parameter equations for the lines ℓ_+ and ℓ_- . The result, in matrix form, is

$$\ell_{\pm} : \begin{pmatrix} \bar{x} \\ \bar{y} \\ \bar{z} \end{pmatrix} = \begin{pmatrix} 0 \\ 0 \\ h \end{pmatrix} + t \begin{pmatrix} \pm\sqrt{2} \\ \sin \gamma \\ \cos \gamma \end{pmatrix}, \quad -\infty < t < \infty, \quad (16)$$

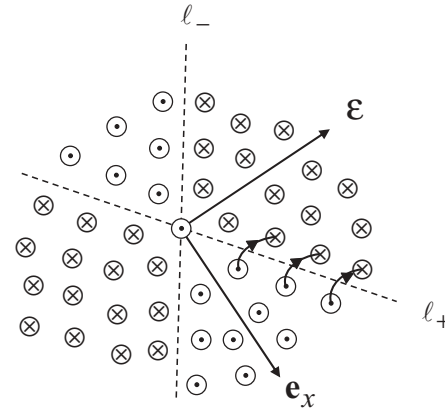


FIG. 4. The plane through the dipole, which is perpendicular to \mathbf{e}' . It follows from Fig. 3 that the plane is spanned by vectors \mathbf{e} and \mathbf{e}_x , and the view is such that \mathbf{e}' is out of the page. The Poynting vector in this plane is perpendicular to the plane, indicated by \otimes and \odot . The Poynting vector $\sigma(\mathbf{q})$ has an overall factor of $v(h) \sin \gamma$, and the orientation is shown for the case where this factor is negative (as in Fig. 5). The Poynting vector changes direction across the lines ℓ_+ and ℓ_- , and this gives rise to a rotation of the field lines around these semisingular lines. This is shown schematically for the ℓ_+ line. For a field point on the \mathbf{e}' axis we have $\cos \alpha = 0$, and it then follows from Eq. (13) that $\sigma(\mathbf{q})$ is in the \mathbf{e}' direction for $v(h) \sin \gamma < 0$. Therefore, at the origin of the plane, the Poynting vector is out of the page.

where $\bar{x} = k_0 x$, $\bar{y} = k_0 y$, and $\bar{z} = k_0 z$ are the dimensionless Cartesian coordinates of points on the lines.

V. EMISSION IN THE yz PLANE

The field lines of the Poynting vector are generally curves in three dimensions. For a field point in the yz plane, however, the Poynting vector is in the yz plane, and therefore the field lines are 2D curves in the yz plane. The vortices from Fig. 5 become closed loops when in the yz plane, as shown by the dashed curves in Fig. 5. Figure 6 shows field lines in the yz

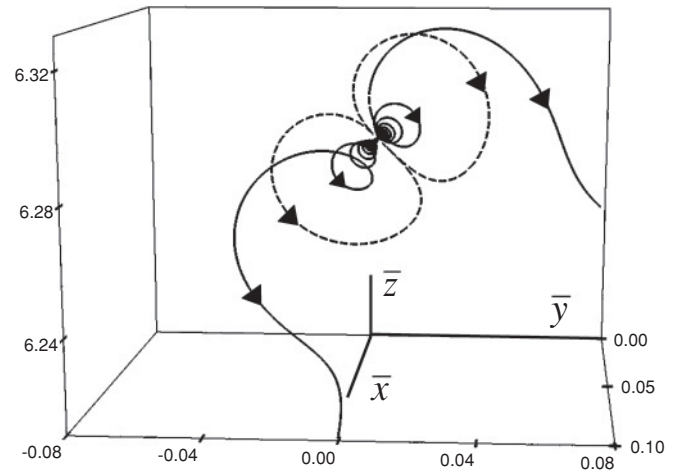


FIG. 5. The field lines of the Poynting vector for electric dipole radiation emitted near a mirror exhibit a vortex structure. Field lines are shown for $\gamma = \pi/4$ and $h = 2\pi$. In the region $x > 0$, the field lines (solid curves) swirl around the semisingular lines of Fig. 4. The dashed field lines are in the yz plane, and they are closed loops.

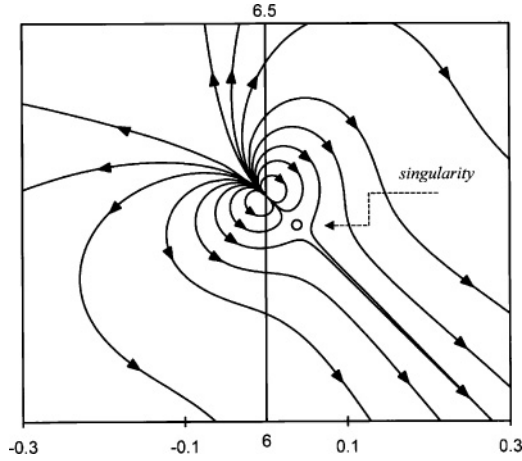


FIG. 6. Field lines of the Poynting vector for a dipole oscillating under 45° with the z axis and located at a distance $h = 2\pi$ above the mirror. The z axis is up and the y axis is to the right. Very close to the dipole the field lines are closed loops, and just below the dipole a singularity appears.

plane (obtained with the exact solution of Appendix A) on a larger scale. The inner two loops are the same as the dashed loops of Fig. 5. Vector $\boldsymbol{\varepsilon}$ (not shown) is under 45° with the z axis, and we see that in the neighborhood of the dipole all field lines cross the $\boldsymbol{\varepsilon}$ axis under 90° and run in the same direction, as expected from Fig. 4. All field lines along the $\boldsymbol{\varepsilon}$ axis in Fig. 4 go into the page, except for the field line through the origin, which comes out of the page. The result is that in Fig. 6 all field lines come out of the dipole along the $\boldsymbol{\varepsilon}'$ axis. In the yz plane, all radiation is emitted in the same direction, which is the direction perpendicular to the direction of oscillation of the dipole. This in sharp contrast to emission in free space for which radiation is emitted in all directions (except along the dipole axis).

The field lines near the dipole form closed loops. This means that the energy propagating along these field lines returns to the dipole at the other side. The closed loops do not contribute to the overall emitted power, but they give a circulation of power in the near field. This situation is reminiscent of the case of two oscillating dipoles close together, where energy is emitted by one dipole and subsequently this energy is absorbed by the other dipole [8]. For that case, field lines run from one dipole to the other, and this mechanism does not contribute to the overall emitted power either.

At a larger distance from the dipole, the free-dipole term $\hat{\mathbf{q}}_1 \sin^2 \alpha$ will eventually become larger than the $O(1/q_1)$ term, and the field lines will run outward. Since just below the dipole in Fig. 6 the field lines run into the dipole, we expect a singularity along the $\boldsymbol{\varepsilon}'$ axis in this area. For a field point on the $\boldsymbol{\varepsilon}'$ axis we have $\alpha = \pi/2$. The Poynting vector of Eq. (13) becomes

$$\boldsymbol{\sigma}(\mathbf{q}) = \hat{\mathbf{q}}_1 - \frac{\sin \gamma}{q_1} v(h) \boldsymbol{\varepsilon}' + O(1), \quad (17)$$

where the first term, $\hat{\mathbf{q}}_1$, is the free-dipole term. At a singularity, the Poynting vector vanishes, and when neglecting the $O(1)$ term, this occurs at the field point

$$\mathbf{q}_1 = \boldsymbol{\varepsilon}' v(h) \sin \gamma. \quad (18)$$

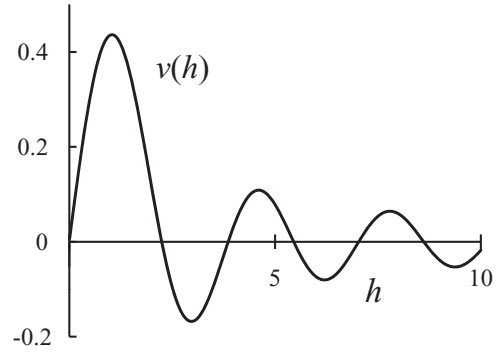


FIG. 7. The leading term of the Poynting vector in the near field is proportional to the function $v(h)$ from Eq. (14), which is shown in this graph. This function determines the dependence of this term on the distance between the dipole and the mirror.

This point is on the $\boldsymbol{\varepsilon}'$ axis and indicated by a little circle in Fig. 6. Equation (18) gives the distance between the singularity and the dipole as $|v(h) \sin \gamma|$. We can view this distance as a measure for the spatial extent of the loops in the very near field of the dipole. For $\gamma = 0$ this distance is zero, because the $O(1/q_1)$ term is absent. So for a dipole oscillating along the z axis there are no loops. For $\gamma \neq 0$, the size of the loops is determined by the function $v(h)$ of Eq. (14), and the graph of this function is shown in Fig. 7. For large h , this function falls off as $\sim 1/h$; therefore, the radial extension of the loops is about $q_1 \lesssim 1/h$. Consequently, when the distance between the dipole and the mirror increases, the loops diminish in size. At a root of $v(h)$ the loops vanish, and when $v(h)$ reverses sign, the field lines of the loops reverse direction. In that case, the singularity appears at the top side of the dipole, rather than below it as in Fig. 6.

For small h we have

$$v(h) = \frac{2h}{3} + O(h^3), \quad (19)$$

so for $h \rightarrow 0$ this function goes to zero. The $O(1/q_1)$ term, which is responsible for the loops, is proportional to $v(h)$, and therefore the loops disappear when the distance h between the dipole and the mirror vanishes. In the limit $h \rightarrow 0$, the exact solution of Appendix A can be simplified, and the result is

$$\boldsymbol{\sigma}(\mathbf{q}) = 4\hat{\mathbf{q}} \cos^2 \gamma \cos^2 \theta, \quad (20)$$

which holds in three dimensions. The Poynting vector is proportional to the radial unit vector $\hat{\mathbf{q}}$ at all distances; therefore, the field lines are straight lines. For $h \rightarrow 0$, the loops and the singularity disappear, and the four vortices from the previous section are not present either.

VI. FIELD LINES IN THE yz PLANE

The pattern of energy emission in the yz plane is illustrated in Fig. 6, showing that the field lines either form closed loops or bend somewhat and then run away from the dipole. It can be seen from the scale in the figure that this pattern is of a very subwavelength nature. Figure 8 shows a larger view of the field lines of energy transport near the mirror. The details of the flow lines of Fig. 6 cannot be resolved on the scale of Fig. 8. Field lines that run downward from the dipole approach the

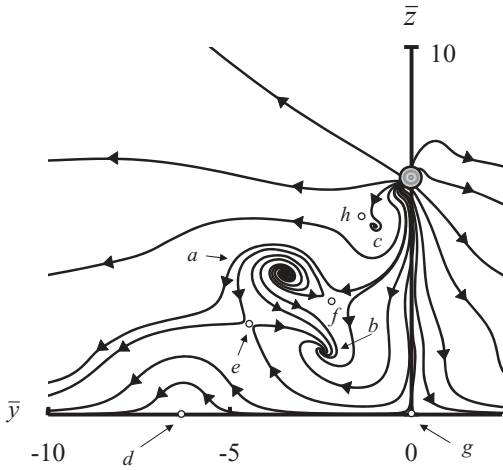


FIG. 8. Field lines of the Poynting vector in the yz plane for a dipole located at a distance of one wavelength from the mirror ($h = 2\pi$), oscillating under an angle of 45° with the z axis ($\gamma = \pi/4$). We observe a complex flow line pattern with singularities and vortices.

mirror (the xy plane), and an intricate field line pattern appears due to interference between the source field and the reflected field. We observe numerous singularities and three vortices for the parameters chosen for the figure ($\gamma = \pi/4, h = 2\pi$). To the right of the z axis and above the dipole (not shown), the field lines are typically smooth curves without any interesting structure, although exceptions are possible. The existence of optical vortices resulting from interference between radiation and its reflection at a surface was predicted for the first time by Braunbek and Laukien for the reflection of a plane wave by the Sommerfeld half-plane [9]. The most common optical vortices are vortices in Laguerre-Gaussian laser beams [10–13], and their structure is related to the angular momentum carried by the beam. Another type of optical vortex is the rotation in the field lines of the Poynting vector of a multipole field [14,15]. These vortices are due to the emission mechanism of the source rather than interference.

Points a , b , and c in Fig. 8 are singularities at the centers of vortices, and the other named points, except for point d , are regular singularities where field lines abruptly change direction. Interestingly, there are field lines that start at vortex a and end at vortex b . These field lines represent a local energy flow where the energy does not directly originate from the location of the dipole. Field lines emanating from vortex a either end in vortex b or they run to the far field, and field lines ending at vortex b either come from vortex a or from the dipole. Other field lines coming from the dipole swing around either vortex a or vortex b and then run to the far field. At point e , some of these field lines seem to collide, and this leads to the singularity at point e . At the singularities f and g , field lines split in two directions. An enlargement of the very small vortex at point c is shown in Fig. 9. Since the field lines split just above the vortex, there has to be a singularity in that region, which is point h .

For other parameter values a similar pattern is observed, and typically the number of singularities and vortices increases with h . An exception is $\gamma = 0$, for which there are no singularities except for the point directly below the dipole,

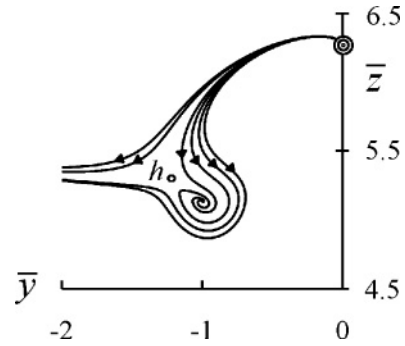


FIG. 9. Enlargement of the vortex c of Fig. 8. At the center of the vortex is a singularity, and very nearby is the singularity labeled h .

at the mirror surface. For this case of a perpendicular dipole, all field lines more or less bend at the mirror as in Fig. 1(b), and this is illustrated in Fig. 10. The field line pattern for a parallel dipole ($\gamma = \pi/2$) is shown in Fig. 11, and we see that there are fewer singularities than in Fig. 8, where the dipole oscillates under 45° with the z axis.

At a singularity the Poynting vector is zero. This can be a result of $\mathbf{E}(\mathbf{r}) = \mathbf{0}$, $\mathbf{B}(\mathbf{r}) = \mathbf{0}$, or $\mathbf{E}(\mathbf{r}) \times \mathbf{B}(\mathbf{r})^*$ imaginary. Since \mathbf{e} and \mathbf{e}^{im} are in the yz plane, it follows from Eq. (4) that $\mathbf{B}(\mathbf{r})$ only has an x component for a field point \mathbf{r} in the yz plane. The amplitude $\mathbf{B}(\mathbf{r})$ is complex, so for $\mathbf{B}(\mathbf{r})$ to vanish it has to hold that both the real and the imaginary parts of the x component have to vanish simultaneously. Working out the expression for $B_x(\mathbf{r})$ gives

$$\frac{\sin q_1 - q_1 \cos q_1}{q_1^3} [\bar{y} + (h - \bar{z}) \tan \gamma] + \frac{\sin q_2 - q_2 \cos q_2}{q_2^3} [\bar{y} + (h + \bar{z}) \tan \gamma] = 0 \quad (21)$$

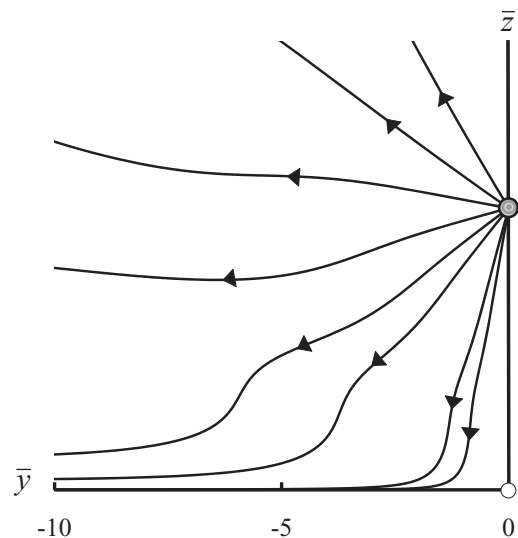


FIG. 10. Field line pattern for a dipole oscillating perpendicular to the plane of the mirror at a distance $h = 2\pi$. For this case, there are no vortices or singularities, except for the point directly below the dipole at the mirror surface. The field line pattern is reflection-symmetric with respect to the z axis.

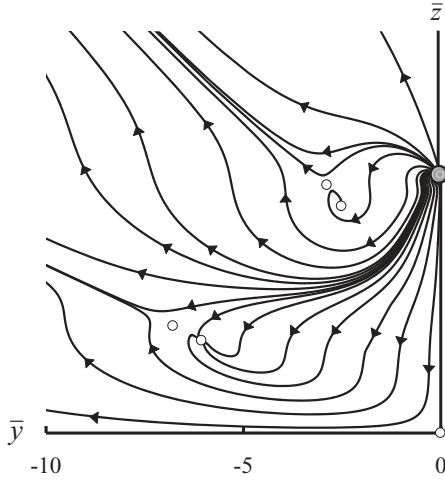


FIG. 11. For a dipole oscillating parallel to the surface at a distance $h = 2\pi$, several singularities appear and they are indicated by small open circles. The energy flow pattern is reflection-symmetric with respect to the z axis.

for $\text{Re}B_x(\mathbf{r}) = 0$ and

$$\frac{\cos q_1 + q_1 \sin q_1}{q_1^3} [\bar{y} + (h - \bar{z}) \tan \gamma] + \frac{\cos q_2 + q_2 \sin q_2}{q_2^3} [\bar{y} + (h + \bar{z}) \tan \gamma] = 0 \quad (22)$$

for $\text{Im}B_x(\mathbf{r}) = 0$, and here $q_1 = \sqrt{\bar{y}^2 + (\bar{z} - h)^2}$ and $q_2 = \sqrt{\bar{y}^2 + (\bar{z} + h)^2}$. Equations (21) and (22) define two sets of curves in the yz plane, and at any intersection the magnetic field is zero. These curves are shown in Fig. 12, and we see that the curves intersect at the location of the three vortices in Fig. 8. Therefore, the vortices are due to the disappearance of the magnetic field at these points. We have verified numerically that at the other singularities $\mathbf{E}(\mathbf{r}) \times \mathbf{B}(\mathbf{r})^*$ is imaginary, except for point d , where we again have $\mathbf{B}(\mathbf{r}) = \mathbf{0}$.

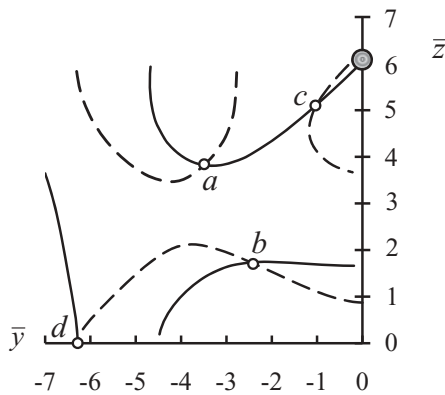


FIG. 12. The solutions of $\text{Re}B_x = 0$ and $\text{Im}B_x = 0$ are indicated by the solid and dashed curves, respectively, and the parameters for this graph are the same as for Fig. 8. At an intersection the Poynting vector is zero, and the intersections a , b , and c correspond to the three vortices in Fig. 8.

VII. FIELD LINES IN THE PLANE OF THE MIRROR

Singularity d in Fig. 8 appears to be of a different nature than the other singularities. There is no vortex at this point, no splitting of the field lines, and no collision between field lines running in different directions (such as at singularity e). Point d is in the surface of the mirror, and field lines in the neighborhood have the appearance of jumping over a bump. Singularity g in Fig. 8 is also in the plane of the mirror, and it can be verified easily from the explicit expressions in Appendix A that $\sigma(\mathbf{q}) = \mathbf{0}$ at the origin of coordinates. For a point in the plane of the mirror, the Poynting vector is in the xy plane and, therefore, field lines through any point in the mirror surface are 2D curves in the mirror plane. In the plane of the mirror we have $q_1 = q_2$, and expression (A11) for $\sigma(\mathbf{q})$ simplifies considerably. When we introduce the vector

$$\mathbf{v} = -\mathbf{e}_y h \tan \gamma, \quad (23)$$

the Poynting vector at the point in the xy plane with position vector \mathbf{q} can be expressed as

$$\sigma(\mathbf{q}) = \frac{4 \cos \gamma}{q_1} \left(\cos \gamma + \frac{h}{q_1} \cos \alpha \right) (\mathbf{q} - \mathbf{v}). \quad (24)$$

Vector \mathbf{v} represents a point on the negative y axis (for $\tan \gamma > 0$), and for $\mathbf{q} = \mathbf{v}$ this gives $\sigma(\mathbf{q}) = \mathbf{0}$. Therefore, the singularity d in Fig. 8 has \mathbf{v} as position vector, and so the \bar{y} coordinate of this point equals $-h \tan \gamma$. The Poynting vector is proportional to $\mathbf{q} - \mathbf{v}$, which is the position vector \mathbf{q} with respect to the singular point \mathbf{v} . So the Poynting vector everywhere in the xy plane is straight out from point \mathbf{v} and, therefore, the field lines are straight lines coming out of or running toward point \mathbf{v} .

With some manipulations of the expressions in Appendix A, we find

$$\cos \alpha = \frac{\cos \gamma}{q_1} (\mathbf{e}_y \cdot \mathbf{q} \tan \gamma - h), \quad (25)$$

and combination with Eq. (24) yields the expression

$$\sigma(\mathbf{q}) = \frac{4 \cos^2 \gamma}{q_1^3} [\mathbf{q} \cdot (\mathbf{q} - \mathbf{v})] (\mathbf{q} - \mathbf{v}) \quad (26)$$

for the Poynting vector. In this form we see immediately that $\sigma(\mathbf{q})$ vanishes at the origin of coordinates, and this is singularity g from Fig. 8. Furthermore, the factor $\mathbf{q} \cdot (\mathbf{q} - \mathbf{v})$ is zero when vector \mathbf{q} is perpendicular to vector $\mathbf{q} - \mathbf{v}$. As can be seen most easily from Fig. 13, this defines a circle in the xy plane. For any \mathbf{q} on this circle, we have $\sigma(\mathbf{q}) = 0$; therefore, this is a singular circle. Across this circle, the Poynting vector changes sign and the field lines change direction. All field lines are straight and go through point \mathbf{v} on the y axis. Outside the singular circle, the angle between \mathbf{q} and $\mathbf{q} - \mathbf{v}$ is less than 90° , so $\mathbf{q} \cdot (\mathbf{q} - \mathbf{v}) > 0$, and therefore $\sigma(\mathbf{q})$ is in the outward direction. Consequently, inside the circle the field lines run from the circle toward the singularity at point \mathbf{v} , and this gives the field line diagram shown in Fig. 14.

For a dipole oscillating along the z axis, we have $\gamma = 0$, and the circle shrinks to a point at the origin of the coordinates. Then all field lines run radially outward from the origin. For a dipole oscillating along the y axis, we have $\gamma \rightarrow \pi/2$, and the radius of the circle goes to infinity. Vector \mathbf{v} becomes

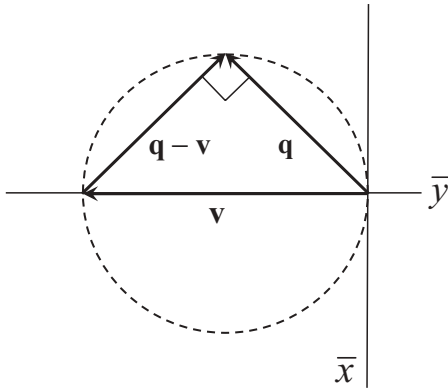


FIG. 13. A field point in the xy plane is represented by the position vector \mathbf{q} with respect to the origin of coordinates. Vector \mathbf{v} is a fixed vector, directed along the y axis, and the same field point can be represented by the position vector $\mathbf{q} - \mathbf{v}$ with respect to the end point of vector \mathbf{v} . The set of all field points that satisfy the equation $\mathbf{q} \cdot (\mathbf{q} - \mathbf{v}) = 0$ then form the circle that is shown, since this equation implies that the angle between \mathbf{q} and $\mathbf{q} - \mathbf{v}$ is 90° .

undefined, and this limit has to be considered more carefully. We find

$$\sigma(\mathbf{q}) = \frac{4h^2}{q_1^3} \bar{y} \mathbf{e}_y. \quad (27)$$

The field lines are parallel to the y axis and the x axis is a singular line. All field lines start at a point on the x axis and run parallel to the y axis to the left and right. This is the limit of Fig. 14, where the circle stretches out so that it becomes the x axis.

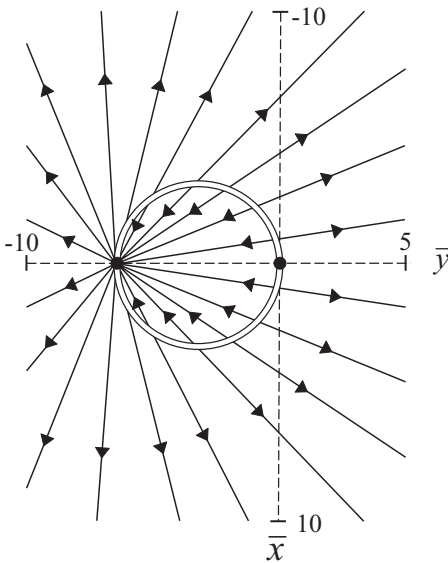


FIG. 14. Field lines in the plane of the mirror (for $\tan \gamma > 0$). The two black dots on the y axis are the singularities d and g from Fig. 8, which are located at point \mathbf{v} and the origin, respectively. In the xy plane, these singularities appear to be the intersections of a singular circle with the y axis. The diameter of the circle is the magnitude of vector \mathbf{v} , which is $h|\tan \gamma|$. When viewed from outside the circle, all field lines appear to come from the singularity at point \mathbf{v} , but inside the circle all field lines run toward the singularity. For $\tan \gamma < 0$, the circle is located in the region $\bar{y} > 0$.

The inside of the circle becomes the region $y < 0$, and all field lines run to the point \mathbf{v} , which is now at $y = -\infty$ on the y axis.

VIII. CONCLUSIONS

When an oscillating electric dipole emits radiation in the vicinity of a mirror, the pattern of energy emission is determined by interference between the electric field of the dipole and the magnetic field of the reflected radiation. The field lines of energy flow form a set of four optical vortices, two of which are shown in Fig. 5. The field lines spiral around two semisingular lines through the dipole, and these lines are oriented as shown in Fig. 4. Their directions are determined by angle γ , which is the angle between the oscillation direction of the dipole and the z axis. The pattern is symmetric under reflection in the yz plane. In the yz plane, these vortices reduce to closed loops, as shown in Fig. 6. It is also found that for emission in the yz plane all energy is emitted in a single direction, which is perpendicular to the dipole. This is in contrast to the emission in free space, where energy is emitted in all directions. Some of the emitted energy propagates along a closed loop, and so it returns to the dipole. Since at a larger distance all energy radiates away from the source, there has to be a singular point near the dipole, as shown in Fig. 6. The location of this point is approximately given by Eq. (18). The function $v(h)$ in this equation goes to zero with increasing h , so when the distance between the dipole and the surface of the mirror becomes larger, the singularity moves closer to the dipole and, hence, the dimension of the loops becomes smaller.

Figure 8 shows the field line pattern in the yz plane from a larger view. We find that numerous singularities are present in the flow line pattern and there are three vortices (for the parameters in the figure). The vortices are due to the vanishing of the magnetic field at the centers of the vortices. Of particular interest is singularity d in the figure. It was shown that this singularity is a point on a singular circle in the plane of the mirror. Inside this circle, the field lines run from a point on the circle to singularity d , and outside the circle they run from a point on the circle to the far field, such that the field lines appear to come from singularity d . Also, in the plane of the mirror, all field lines are straight, as follows from Eq. (24).

When subwavelength resolution of the energy flow is taken into consideration, the interference pattern between the dipole radiation and its own reflection from a mirror is far from trivial. A ray diagram as in Fig. 1(a) or an educated guess as in Fig. 1(b) are not even close to the intricate pattern of energy flow that appears in this simple system. Particularly fascinating is the fact that for a linear dipole the radiation is emitted as a set of four vortices, except when the dipole oscillates exactly perpendicular to the mirror. For a realistic metal surface, rather than an ideal mirror, this emission pattern will be very similar since the effect is due to interference between the radiation emitted by the dipole and the reflected field. The field reflected by the mirror is finite at the location of the dipole; therefore, the four-vortex structure will be present in the emission pattern near any reflecting surface.

APPENDIX A

The Poynting vector for electric dipole radiation near a mirror can be evaluated explicitly, as outlined in Sec. III. In

terms of the parameters

$$a = \boldsymbol{\varepsilon} \cdot \hat{\mathbf{q}}_1, \quad (\text{A1})$$

$$a' = \boldsymbol{\varepsilon}^{\text{im}} \cdot \hat{\mathbf{q}}_1, \quad (\text{A2})$$

$$b = \boldsymbol{\varepsilon}^{\text{im}} \cdot \hat{\mathbf{q}}_2, \quad (\text{A3})$$

$$b' = \boldsymbol{\varepsilon} \cdot \hat{\mathbf{q}}_2, \quad (\text{A4})$$

$$c = \hat{\mathbf{q}}_1 \cdot \hat{\mathbf{q}}_2, \quad (\text{A5})$$

$$c' = \boldsymbol{\varepsilon} \cdot \boldsymbol{\varepsilon}^{\text{im}}, \quad (\text{A6})$$

and the functions

$$f_1 = \left[1 - \frac{i}{q_1} \left(1 - \frac{i}{q_1} \right) \right] \left(1 + \frac{i}{q_2} \right), \quad (\text{A7})$$

$$g_1 = \left[1 - \frac{3i}{q_1} \left(1 - \frac{i}{q_1} \right) \right] \left(1 + \frac{i}{q_2} \right), \quad (\text{A8})$$

$$f_2 = \left[1 + \frac{i}{q_2} \left(1 + \frac{i}{q_2} \right) \right] \left(1 - \frac{i}{q_1} \right), \quad (\text{A9})$$

$$g_2 = \left[1 + \frac{3i}{q_2} \left(1 + \frac{i}{q_2} \right) \right] \left(1 - \frac{i}{q_1} \right), \quad (\text{A10})$$

the Poynting vector takes the form

$$\boldsymbol{\sigma}(\mathbf{q}) = (1 - a^2)\hat{\mathbf{q}}_1 + \left(\frac{q_1}{q_2} \right)^2 (1 - b^2)\hat{\mathbf{q}}_2 + \frac{q_1}{q_2} \text{Re}[e^{i(q_2 - q_1)} \mathbf{Z}], \quad (\text{A11})$$

with

$$\mathbf{Z} = (c'\hat{\mathbf{q}}_2 - b'\boldsymbol{\varepsilon}^{\text{im}})f_1 + a(c\boldsymbol{\varepsilon}^{\text{im}} - a'\hat{\mathbf{q}}_2)g_1 + (c'\hat{\mathbf{q}}_1 - a'\boldsymbol{\varepsilon})f_2 + b(c\boldsymbol{\varepsilon} - b'\hat{\mathbf{q}}_1)g_2. \quad (\text{A12})$$

The first term on the right-hand side of Eq. (A11), proportional to $\hat{\mathbf{q}}_1$, is the Poynting vector for a free dipole (no mirror) and the second term, proportional to $\hat{\mathbf{q}}_2$, would be the Poynting vector of the mirror dipole, if it were a free dipole. The third term in Eq. (A11) is the interference term, involving cross terms between the source field and the reflected field.

The parameters given by Eqs. (A1)–(A6) can be worked out further by using expressions (9) and (10) for $\boldsymbol{\varepsilon}$ and $\boldsymbol{\varepsilon}^{\text{im}}$, respectively. In terms of the polar angles (θ_1, ϕ) with respect to the position of the dipole (Fig. 3), we have

$$\hat{\mathbf{q}}_1 = \mathbf{e}_\rho \sin \theta_1 + \mathbf{e}_z \cos \theta_1, \quad (\text{A13})$$

where

$$\mathbf{e}_\rho = \mathbf{e}_x \cos \phi + \mathbf{e}_y \sin \phi \quad (\text{A14})$$

is the radial unit vector in the xy plane, and it can be seen from Fig. 3 that

$$\hat{\mathbf{q}}_2 = \frac{q_1}{q_2} \left(\hat{\mathbf{q}}_1 + \mathbf{e}_z \frac{2h}{q_1} \right), \quad (\text{A15})$$

with $h = k_0 H$. We then obtain

$$a = \sin \theta_1 \sin \phi \sin \gamma + \cos \theta_1 \cos \gamma, \quad (\text{A16})$$

$$a' = -\sin \theta_1 \sin \phi \sin \gamma + \cos \theta_1 \cos \gamma, \quad (\text{A17})$$

$$b = \frac{1}{q_2} (a' q_1 + 2h \cos \gamma), \quad (\text{A18})$$

$$b' = \frac{1}{q_2} (a q_1 + 2h \cos \gamma), \quad (\text{A19})$$

$$c = \frac{1}{q_2} (q_1 + 2h \cos \theta_1), \quad (\text{A20})$$

$$c' = \cos(2\gamma). \quad (\text{A21})$$

From Eq. (A1) it follows that we also have $a = \cos \alpha$, where α is the angle between $\boldsymbol{\varepsilon}$ and $\hat{\mathbf{q}}_1$.

APPENDIX B

Close to the dipole, the parameter q_1 is small, and the expressions from Appendix A can be simplified. We assume that $q_1 \ll 1$ and $q_1 \ll h$. It follows from Eqs. (A15) and (A13) that the magnitude of vector \mathbf{q}_2 is

$$q_2 = \sqrt{q_1^2 + 4hq_1 \cos \theta_1 + 4h^2}, \quad (\text{B1})$$

and, therefore,

$$q_2 = 2h + q_1 \cos \theta_1 + O(q_1^2). \quad (\text{B2})$$

This function of q_1 appears in f_1 , g_1 , f_2 , and g_2 of Eqs. (A7)–(A10), in the parameters b , b' , and c of Eqs. (A18)–(A20), and in the interference term in Eq. (A11). The unit vector in the \mathbf{q}_2 direction, appearing on the right-hand side of Eq. (A12), becomes

$$\hat{\mathbf{q}}_2 = \mathbf{e}_z + \frac{q_1}{2h} \mathbf{e}_\rho \sin \theta_1 + O(q_1^2). \quad (\text{B3})$$

A systematic expansion in orders of q_1 then yields for the Poynting vector in the near field

$$\begin{aligned} \boldsymbol{\sigma}(\mathbf{q}) = & \hat{\mathbf{q}}_1 \sin^2 \alpha + \sin \gamma \left[\frac{v(h)}{q_1} + w(h) \cos \theta_1 \right] \\ & \times [(3a^2 - 1)\boldsymbol{\varepsilon}' - 3a(\hat{\mathbf{q}}_1 \cdot \boldsymbol{\varepsilon}')\boldsymbol{\varepsilon}] \\ & + \sin \gamma \frac{\sin(2h)}{2h} (\boldsymbol{\varepsilon} \sin \theta_1 \sin \phi - \hat{\mathbf{q}}_1 \sin \gamma) \\ & + \frac{v(h)}{2h} [\mathbf{e}_\rho (c' - 3aa') \sin \theta_1 - \hat{\mathbf{q}}_1 (c' - 3\cos^2 \gamma) \\ & + \boldsymbol{\varepsilon}^{\text{im}} (3a \sin \theta_1 - \sin \gamma \sin \phi) \sin \theta_1 \\ & - \boldsymbol{\varepsilon} (3 \cos \gamma \cos \theta_1 - a')] + O(q_1). \end{aligned} \quad (\text{B4})$$

Here, $v(h)$ and $\boldsymbol{\varepsilon}'$ are defined in Sec. IV, and in addition we introduce the function

$$w(h) = \frac{1}{2h^2} \cos(2h) + \frac{1}{2h} \left(1 - \frac{1}{2h^2} \right) \sin(2h). \quad (\text{B5})$$

[1] M. Born and E. Wolf, *Principles of Optics*, 6th ed. (Pergamon, Oxford, 1980), Chap. 3.

[2] A. J. Devaney and E. Wolf, *Opt. Commun.* **9**, 327 (1973).

[3] J. Gasper, G. C. Sherman, and J. J. Starnes, *J. Opt. Soc. Am.* **66**, 955 (1976).

[4] L. Mandel and E. Wolf, *Optical Coherence and Quantum Optics* (Cambridge University, Cambridge, England, 1995), p. 120.

[5] H. F. Arnoldus and J. T. Foley, *J. Opt. Soc. Am. A* **21**, 1109 (2004).

- [6] J. D. Jackson, *Classical Electrodynamics*, 3rd ed. (Wiley, New York, 1999), p. 411.
- [7] H. F. Arnoldus, *J. Mod. Opt.* **54**, 45 (2007).
- [8] S. Maeda and P. Diamant, *IEEE Ant. Prop.* **44**, 68 (2002).
- [9] W. Braunbek and G. Laukien, *Optik* **9**, 174 (1952).
- [10] M. Vasnetsov and K. Staliunas eds., *Optical Vortices, Horizons in World Physics*, Vol. 228 (Nova Science, New York, 1999).
- [11] A. V. Volyar, V. G. Shvedov, and T. A. Fadeeva, *Opt. Spectrosc.* **90**, 93 (2001).
- [12] V. A. Pas'co, M. S. Soskin, and M. V. Vasnetsov, *Opt. Commun.* **198**, 49 (2001).
- [13] A. V. Volyar, T. A. Fadeeva, and V. G. Shvedov, *Opt. Spectrosc.* **93**, 267 (2002).
- [14] H. F. Arnoldus and J. T. Foley, *Opt. Commun.* **231**, 115 (2004).
- [15] H. F. Arnoldus, *Opt. Commun.* **252**, 253 (2005).